Hindawi
Advances in Materials Science and Engineering
Volume 2020, Article ID 9027534, 11 pages
https://doi.org/10.1155/2020/9027534

Research Article

High-Temperature Tensile Fractography of Zr-, Ni-, and Mn-Containing Al-Si-Cu-Mg Cast Alloys

M. H. Abdelaziz,[1,2] **E. M. Elgallad**,[1] **A. M. Samuel**,[1] **H. W. Doty**,[3] **and F. H. Samuel**[1]

[1]*Département des Sciences Appliquées, Université du Québec à Chicoutimi, Saguenay, Canada*
[2]*Département PEC, Université Française d'Égypte, Ville Shorouk, Le Caire, Egypt*
[3]*General Motors Materials Engineering, 823 Joslyn Ave, Pontiac, MI 48340, USA*

Correspondence should be addressed to M. H. Abdelaziz; mohamed.abdelaziz1@uqac.ca

Received 16 December 2019; Revised 24 February 2020; Accepted 3 March 2020; Published 9 April 2020

Academic Editor: Akbar Heidarzadeh

This study investigated the fracture behavior of 0.3% Zr-containing 354 alloy following the addition of 0.75% Mn or 2%Ni. The examined surfaces were obtained from tensile testing of the bars at 250°C. For each alloy, the test bar samples were examined in the T6-treated conditions after being exposed to 250°C for 1 and 200 hours. The fracture surface of the base alloy (0.3% Zr-containing 354 alloy) after stabilization for one hour at 250°C reveals a dimpled structure throughout, indicating the ductile nature of the fracture mode. The Al_x (Zr, Ti)Si complex compound is observed with star-like and blocky morphologies, with cracks appearing in various particles of this compound. By increasing the stabilization time up to 200 hours, coarser and deeper dimples are formed, highlighting the increased ductility of the alloy due to the softening behavior associated with the prolonged exposure at 250°C. In the one-hour stabilized T6-treated condition alloy containing 2% Ni tested at 250°C, the appearance of microcracks in the Ni-rich phases and the lower density of dimples on the fracture surface compared to those observed in the base alloy emphasize the low ductility of alloy due to Ni-containing intermetallics. Examination of the fracture surface of Mn-containing alloys revealed the advantageous role of sludge particles in resisting the propagation of cracks that developed in many intermetallic phases.

1. Introduction

Among the category of Al-Si alloys, there are three major alloy systems in the 3xxx series, i.e., Al-Si-Mg, Al-Si-Cu, and Al-Si-Cu-Mg systems. The 354-type alloy belongs to the Al-Si-Cu-Mg system, along with the well-known B319 alloy. Permanent mold-cast 354-type alloys display superior mechanical properties after the application of appropriate heat treatment procedures. The anticipated improvement in the mechanical properties is owed to the presence of both copper (Cu) and magnesium (Mg) as hardening elements [1–4]. In this alloy system, iron is considered as an impurity. It was reported that in Al-Si alloys, if the iron content increases, the mechanical properties, particularly the ductility, will be significantly reduced due to the formation of the brittle β-Al_5FeSi phase [5, 6]. The addition of manganese (Mn) to Fe-containing aluminum alloys is a practice commonly used to neutralize the negative effects of Fe. The addition of Mn will promote the formation of the less harmful α-iron AlFeMnSi phase with Chinese script-like morphology; which will, in turn, improve the overall mechanical properties of Al-alloys [6–8].

Nam and Lee [9], Lee et al. [10], and Park and Nam [11] reported that the addition of 0.5 wt% or higher levels of Mn to Al alloys will enhance the strength values significantly without affecting the ductility. The same trend was also observed by Garza-Elizondo [12] with the addition of 0.75 wt% Mn to Al-Si-Cu-Mg alloys. The increased amount of Mn in Al-Si-Cu-Mg alloys resulted in the transformation of the β-phase needles into α-phase in script-like form and as large polygonal particles. These large particles were similar in morphology to the commonly known sludge particles, however, without Cr. Thus, Garza-Elizondo [12] concluded that the presence of these

large particles, termed as sludge, is not necessarily harmful to the mechanical properties as is commonly reported in the literature; the same conclusion was also reported earlier by Samuel et al. [13].

Many studies [14–22] have been carried out in the past decade on how to maintain the mechanical properties of aluminum alloys at service temperatures that exceed 200°C. Among these, the addition of small amounts of transition metals was found to be a promising approach to maintain the mechanical properties of aluminum alloys at temperatures of up to 300°C. As the addition of transition elements was shown to be beneficial from the point of view of enhancing the precipitation strengthening of trialuminides [23–25], Ni and Mn were added to the Zr-containing Al-Si-Cu-Mg alloy in this study in an attempt to enhance the room- and elevated-temperature mechanical properties of such alloys used in automotive engine components. Thus, Zr was added to the 354 alloy used in this study to form the base or reference alloy, and other elements (Ni and Mn) were subsequently added individually to study their effect with Zr on the fracture behavior of 354 alloy pulled at elevated temperature (250°C).

Abdelaziz et al. [14, 19] studied the mechanical behavior of similar system of alloys and concluded that the addition of Zr, Ni, and Mn enhances the overall mechanical properties of 345 cast alloy including tensile properties at both ambient and 250°C, hardness values, and impact properties. In particular, Abdelaziz et al. [14] stated that the enhancement in mechanical properties of Mn-containing alloys were attributed to the formation of blocky α-Al_{15} (Fe, Mn)$_3Si_2$ and the script-like-α-iron phase. Also, it was stated that [19] the prolonged thermal exposure of alloys containing Zr, Ni, and Mn at 250°C has a detrimental effect on the mechanical properties of the studied alloys owing to the coarsening of the strengthening precipitates.

Based on the aforementioned, the present study will discuss the effect of transition element additions, mainly Mn and Ni, on the elevated-temperature mechanical properties of Zr-containing 354-type alloys after being stabilized at 250°C for one hour and 200 hours before testing. The investigation is mainly dependent on the fracture mechanism of the studied alloys.

2. Experimental Procedure

The base alloy in this research work is 354-type alloy with a minor addition of Zirconium (Zr) (~0.3 wt.%). This alloy was selected based on its improved room- and high-temperature tensile properties as reported in previous studies in the same research group [14, 19].

The as-received 354 alloy ingots were cut, dried, and melted in a 70-Kg capacity SiC crucible using an electric resistance furnace. The melt was kept at a temperature of 800 ± 5°C. This melt superheating was carried out in order to assure the complete melting of all Zr- and Ni-containing compounds from master alloys. The various alloying additions were made using the necessary elements either in pure form or as master alloys. Silicon (Si), copper (Cu), and magnesium (Mg) were added in the form of pure elements, whereas the other alloying elements were added in the form of master alloys.

The studied alloys were Sr-modified by adding ~200 ppm Sr using Al-10 wt.% Sr master alloy, whereas the grain refinement was accomplished through the addition of Al-5 wt.% Ti-1 wt.% B master alloy in the form of rods in order to achieve a level of ~0.2 wt.% Ti in the final alloys. The Mn, Ni, and Zr additions were carried out using Al-25 wt.%Mn, Al-20%Ni, and Al-15%Zr master alloys to achieve the required levels 0.75 wt.% 2% and 0.3%Zr, respectively. Three samplings for chemical analysis were also taken at different times during the casting process in order to ensure the homogeneity of the chemical composition; these samplings were taken at the start, the middle, and the end of the casting process. The chemical analysis was carried out using a Spectrolab-JrCCD Spark Analyzer. The average chemical compositions (three burns per alloy sample) are reported in Table 1.

The addition of master alloys was carried out instantly before starting the degassing process in order to ensure homogeneous mixing of additives during degassing. The degassing process was carried out using a rotary graphite impeller that rotates at ~120 rpm for 15–20 min.; pure dry argon was pumped inside the melt through the rotating impeller at a constant rate of 20 m^3/h. After degassing, the melt was carefully skimmed to remove the oxide layers from the melt surface. The melt was then poured into an ASTM B-108 type permanent mold preheated at 450°C in order to remove all traces of moisture from the mold.

The tensile bars were heat-treated according to the T6-procedure which starts by solution treatment at 495°C for 5 hours, then quenching in warm water at 60°C, and ends up by an artificial aging treatment at 180°C for 8 hours. The tensile bars in the T6-condition were thereafter stabilized at 250°C for various periods of time (1 and 200 hours); in this practice, all bars were placed inside the heat treatment furnace at 250°C and kept for the respective time of exposure.

An Instron Universal mechanical testing machine was used to carry out the tensile testing at elevated temperature (250°C), using a strain rate of 4×10^{-4} s^{-1}. The testing was carried out at 250°C after holding the test bar for half an hour at the testing temperature in order to homogenize the temperature of the sample to 250°C throughout. The test sample was kept unmounted from one side inside the heating chamber during the holding process to avoid compressive stresses that might arise from the expansion of the bar, and then it was mounted from the other side and kept at the testing temperature for another 30 min. A data acquisition system attached to the machine provided the tensile data, namely, the ultimate tensile strength (UTS), the yield strength at 0.2% offset strain (YS), the modulus of elasticity (E), and the percent elongation to fracture (%El), calculated over the gauge length of the test bar. Five test bars were used for each alloy composition/condition studied. The average values of UTS, YS, and %El from each set of five bars were considered as representing the tensile properties of that alloy/condition.

Table 1: Chemical composition of the alloys investigated in this study.

Alloy description		Chemical analysis (wt.%) Elements									
Type	Code	Si	Cu	Mg	Fe	Ti	Zr	Ni	Mn	Sr	Al
354	M1S	8.5	1.76	0.50	0.1	0.2	0.32	<0.1	0.01	0.02	Bal.
	M2S	8.4	1.7	0.60	0.14	0.21	0.33	1.9	0.01	0.02	Bal.
	M3S	8.6	1.8	0.50	0.11	0.25	0.33	<0.1	0.74	0.02	Bal.

The fracture surfaces were extracted from the broken bars, as shown in Figure 1. The fracture surfaces of tensile-tested samples were examined using the same SEM, employing the backscattered electron (BSE) detector and EDS system. The fracture behavior was analyzed using the backscattered electron (BSE) images obtained, and analysis of the EDS spectra of phases observed on the fracture surface was performed.

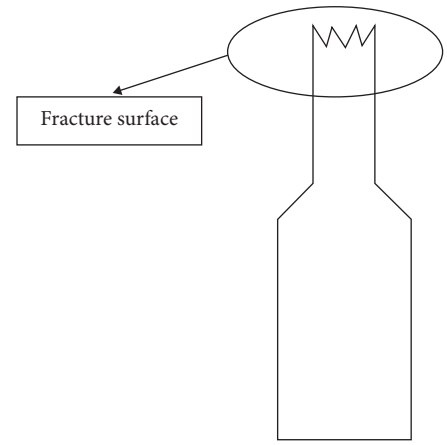

Figure 1: Schematic representation of the location of the fracture surfaces.

3. Results and Discussion

Table 2 presents the tensile properties of the investigated alloys obtained at 250°C for the stabilized T6-treated conditions. An immediately noticeable observation in Table 2 is that the nonstabilized T6-treated conditions of M2S exhibit better strength values (UTS and YS) than those obtained with stabilized T6-treated conditions for each alloy. The ductility values obtained after stabilization conditions are dramatically lower than those obtained after stabilization of T6-treated conditions (cf. 2.26% and 4.57%); without stabilization treatment, the ductility values in the two cases differ by about 0.3% in favor of the T6-treated condition.

The rest of the article shows the results of a detailed investigation of the fracture surfaces of tensile bars of alloys M1S, M2S, and M3S tested at 250°C. For each alloy, the test bar samples were examined in the T6-treated conditions, following two stabilization treatment conditions, corresponding to (i) 1 hour at 250°C and (ii) 200 hours at 250°C. It is important to recall that the T6-temper treatment comprises solution treatment at 495°C for 5 hours followed by quenching in warm water at 60°C and then artificial aging at 180°C for 8 hours. The T6-temper treatment was focused upon, as it is widely used in industry, and hence, understanding the fracture behavior of the alloys in the T6-treated condition would be helpful from the point of view of potential applications.

The BSE image shown in Figure 2(a) reveals the fracture surface of the tensile-tested base alloy M1S in the T6-treated condition and after stabilization for one hour at 250°C. It is noticeable that the fracture surface has a dimpled structure throughout, which indicates the ductile nature of the fracture mode. Additionally, the BSE image reveals the presence of Al_x (Zr, Ti)Si complex compound, as was confirmed by the EDS spectrum in Figure 2(b), appearing in star-like and blocky morphologies; cracks can be spotted in various particles of this complex compound, as indicated by the arrows. The higher magnification BSE image shown in Figure 2(c) displays a cracked Al_x (Zr, Ti)Si phase particle with a blocky morphology. This phase is considered to contribute mainly to the fracture behavior of this alloy by facilitating the crack initiation process. For each of the alloys studied, chemical compositions of phases corresponding to EDS spectra reported in the present work are listed in Table 3.

Additionally, Fe-bearing phases including the π-Al-Si-Mg-Fe and β-Al-Si-Fe phases were detected in the BSE image shown in Figure 3(a) and confirmed by the EDS spectra shown in Figures 3(b) and 3(c), respectively. The arrows point to fine precipitates appearing near the observed intermetallic compounds and away from the dimpled regions on the fracture surface.

Figure 4(a) shows the fracture surface of the T6-treated base alloy M1S tested at 250°C after stabilization for 200 hours at the testing temperature. The dimples in this case are coarser compared to those observed after the one-hour stabilization at 250°C. This highlights the improved ductility of the alloy due to the softening behavior associated with the prolonged elevated-temperature exposure at 250°C. Coarsened precipitates appear in the interiors of the dimples, as indicated by the oval contours in Figure 4(a). The BSE image and the EDS spectrum shown in Figure 4(b) and Figure 4(c), respectively, confirm the presence of Al_x(Zr, Ti)Si phase particles which possibly act as crack initiation sites.

Surappa et al. [26] in their study on the deformation and fracture of A356 alloys suggested that the microcracks which are formed in the intermetallic and the Si particles in rapidly solidified A356 alloys are short and that it is difficult to link them (coalescence) with each other due to the presence of a large ductile α-Al region. As a result, the microcracks linkage may be facilitated by the ductile fracture of the α-Al between the cracked Si particles as illustrated in Figure 5.

Table 2: Tensile properties of the three used alloys tested at 250°C.

Alloy code	Condition	UTS (MPa)	SD	YS (MPa)	SD	%El	SD
M1S (354 + 0.3% Zr)	T6	217.3	6.76	213.7	6.49	1.9	0.25
	T6 + 100 h	95.8	1.22	76.8	0.50	12.1	0.48
	T6 + 200 h	91.6	4.30	78.3	1.44	11.0	0.49
M2S (M1S + 2% Ni)	T6	223.7	8.51	222.3	13.94	2.2	0.08
	T6 + 100 h	102.4	1.63	83.4	2.72	9.4	0.49
	T6 + 200 h	100.7	4.04	80.6	3.33	8.4	0.77
M3S (M1S + 0.75% Mn)	T6	248.7	9.79	245.6	11.07	1.5	0.09
	T6 + 100 h	104.8	5.29	84.3	4.10	12.0	0.83
	T6 + 200 h	101.8	1.45	81.4	1.21	13.5	0.63

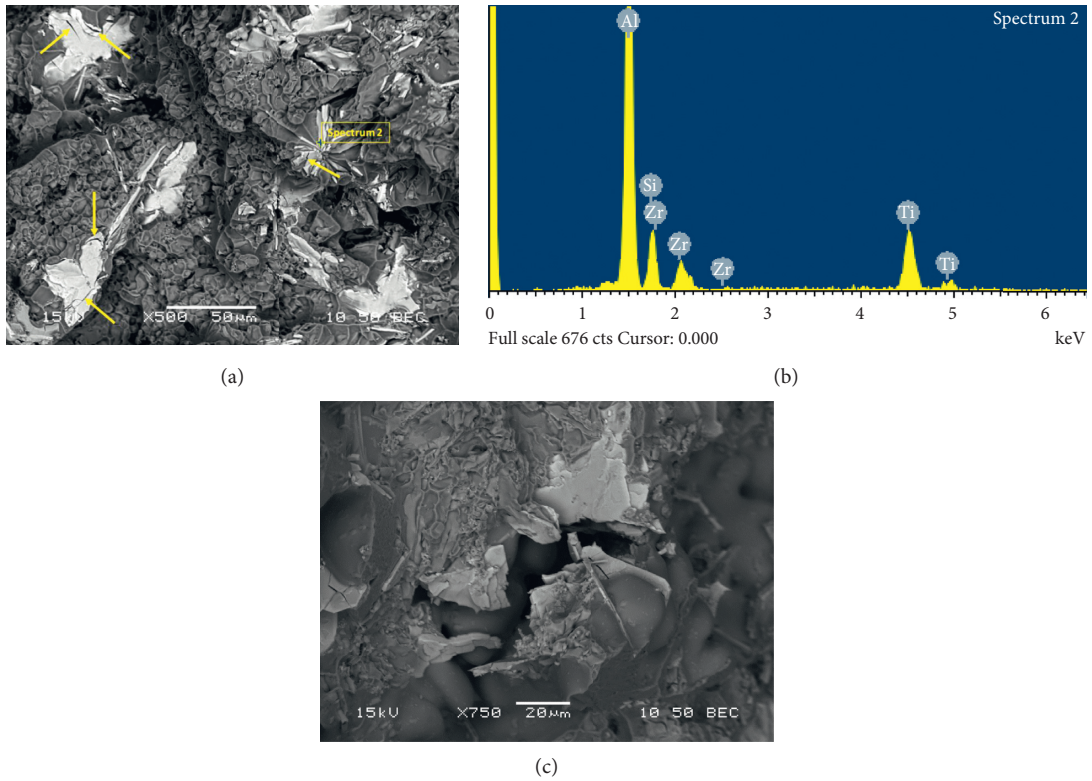

Figure 2: SEM images of T6-treated M1S alloy after stabilization at 250°C for 1 hour: (a) BSE image showing a uniform dimple structure and cracked particles (arrowed), (b) EDS spectrum corresponding to the point of interest in (a), and (c) high magnification BSE image showing a cracked Al-Si-Ti-Zr particle.

The fracture surface of the T6-treated alloy M2S tested at 250°C after one hour of stabilization is shown in Figure 6(a). Microcracks can be observed associated with the Ni-rich phases (solid arrows). The fracture surface exhibits a lower density of dimples compared to that observed in the base alloy M1S after the same treatment/condition; this observation emphasizes the low ductility of the M2S alloy in comparison to alloy M1S. The enhanced ductility of the base alloy over that of alloy M2S can be attributed to the higher volume fraction of intermetallic phases formed in the M2S alloy. The EDS spectrum in Figure 6(b) confirms the presence of Al-Cu-Ni-Fe phase. Figure 7(a) shows a high magnification BSE image of the cracked phase in the circled area in Figure 6(a). This BSE image and the associated EDS spectra shown in Figure 7(b) and Figures 7(c) and 7(d) reveal the presence of multiple cracked Ni-rich phases which are believed to contribute to the crack initiation process.

By increasing the stabilization time at 250°C up to 200 hours for the T6-treated M2S alloy, the dimple nature of the fracture surface, depicted in Figure 8(a), is not very different from that observed after 1 hour of stabilization at 250°C. The fracture surface presents similar features with respect to the presence of Ni-rich phases as those observed in Figure 6(a). The arrows point at some of the shiny particles, which are possibly fine Ni-containing precipitates. The EDS spectra shown in Figure 8(b) and Figure 8(c) confirm the presence of Al-Ni-Fe and Al-Ni-Cu-Fe phases, which are key phases in controlling the fracture behavior of alloy M2S.

The presence of sludge particles in the microstructure of alloy M3S plays a vital role in controlling the tensile

Table 3: Chemical compositions of phases corresponding to EDS spectra reported in the present work.

Figure #	Element	at%	Wt.%
2(b)	Al	60.77	44.42
	Si	13.52	10.28
	Ti	15.56	20.19
	Zr	10.16	25.11
	Mg	15.98	13.81
3(b)	Al	55.20	52.92
	Si	24.49	24.44
	Fe	3.50	6.95
3(c)	Al	69.58	60.70
	Si	17.53	15.92
	Fe	12.45	22.47
	Cu	0.44	0.91
4(c)	Al	59.21	43.41
	Si	14.99	11.44
	Ti	15.99	20.82
	Zr	9.81	24.33
6(b)	Al	78.78	63.28
	Si	0.61	0.51
	Fe	1.29	2.14
	Ni	17.27	30.19
	Cu	2.06	3.89
7(b)	Al	26.20	14.18
	Si	1.36	0.77
	Fe	4.81	5.39
	Ni	67.17	79.09
	Cu	0.45	0.57
7(c)	Al	34.38	19.80
	Si	2.88	1.72
	Fe	3.77	4.50
	Ni	57.98	72.64
	Cu	0.99	1.34
7(d)	Al	16.54	8.35
	Ni	83.18	91.32
	Cu	0.28	0.33
8(b)	Al	80.84	66.36
	Si	0.79	0.68
	Fe	1.35	2.29
	Ni	15.12	27.00
	Cu	1.89	3.66
8(c)	Al	82.23	68.21
	Si	0.57	0.49
	Fe	1.43	2.45
	Ni	13.23	23.88
	Cu	2.54	4.97
	Mg	5.25	4.67
9(b)	Al	88.99	87.89
	Si	4.60	4.73
	Cu	1.16	2.71
9(c)	Al	74.79	65.28
	Si	12.11	11.00
	Mn	10.02	17.80
	Fe	1.73	3.12
10(b)	Al	59.84	43.95
	Si	15.15	11.59
	Ti	14.94	19.48
	Zr	10.06	24.99
10(c)	Al	74.79	65.28
	Si	12.11	11.00
	Mn	10.02	17.80
	Fe	1.73	3.12
	Cu	1.36	2.79
11(b)	Al	60.76	45.06
	Si	15.54	11.99
	Ti	13.83	18.21
	Zr	9.87	24.74

properties and, hence, the fracture behavior of this alloy. The fracture surface of the T6-treated M3S alloy stabilized at 250°C for 1 hour before testing at 250°C is displayed in the BSE image shown in Figure 9(a). The propagation of the branched crack developed in the *Q*-phase ($Al_5Mg_8Cu_2Si_6$) [15], as confirmed by the corresponding EDS spectrum of Figure 9(b), appears to be hindered by the presence of the blocky sludge particle, identified by the associated EDS spectrum shown in Figure 9(c). Similar action of the sludge particles in retarding crack propagation can be noted in Figure 9(d). Yet another interesting observation made from this figure is that, while many of the intermetallic phase particles appear cracked, as indicated by the solid arrows, the sludge particles, however, are crack-free. This observation emphasizes the favorable effect of the presence of sludge particles on the mechanical properties. Besides the sludge particles, the fracture surfaces show noticeable dimpled structure which reflects the good level of ductility experienced by this alloy during tensile testing at 250°C.

Figure 10(a) shows the fracture surface of T6-treated M3S alloy after stabilization for 200 hours at 250°C and tested at the same temperature. The propagation of the crack detected in the star-like Al_x (Zr, Ti)Si phase particle is hindered by the adjacent blocky sludge particle, as depicted in the BSE image shown in Figure 10(a). The corresponding EDS spectra shown in Figure 10(b) and Figure 10(c) confirmed the two phases. The fracture surface Figure 10(a) exhibits coarse and deep dimples because of the improved elevated-temperature ductility of this alloy after applying the stabilization treatment.

Figure 11(a) shows the coarsened precipitates distributed over the fracture surface of the T6-treated M3S alloy after stabilization at 250°C for 200 hours. Thin plates of Al_x(Zr, Ti) Si phase with different orientations are also seen in the BSE image. The corresponding EDS spectrum displayed in Figure 11(b) confirmed these plates to be the Al_x(Zr, Ti)Si phase.

Figure 12 shows the cross sections beneath the fracture surface of M1S alloy. In the T6 condition with UTS~217 MPa and %El~2, several cracks have been observed either through the interdendritic area (referred to by the white arrow in Figure 12(a)) or the intermetallic

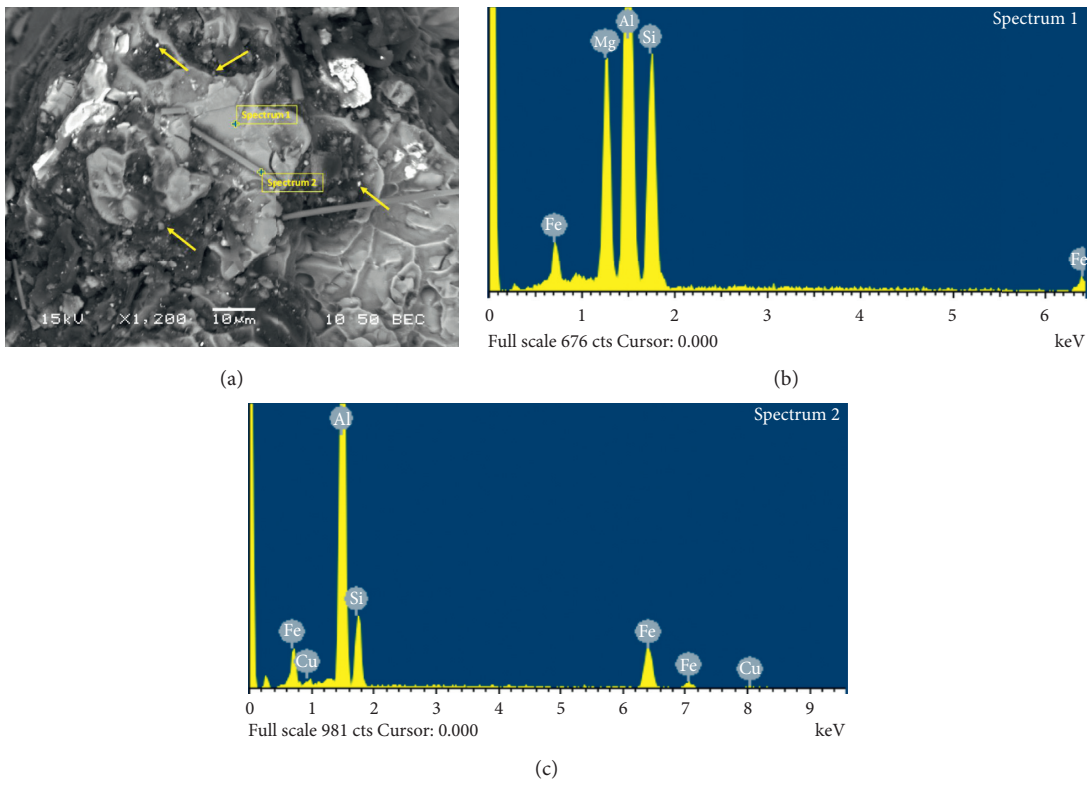

Figure 3: (a) BSE image of T6-treated M1S alloy after stabilization at 250°C for 1 hour showing Fe-bearing phases and (b), (c) EDS spectra corresponding to the points of interest in (a), confirming the presence of π-Al-Si-Mg-Fe, and β-Al-Si-Fe phases, respectively.

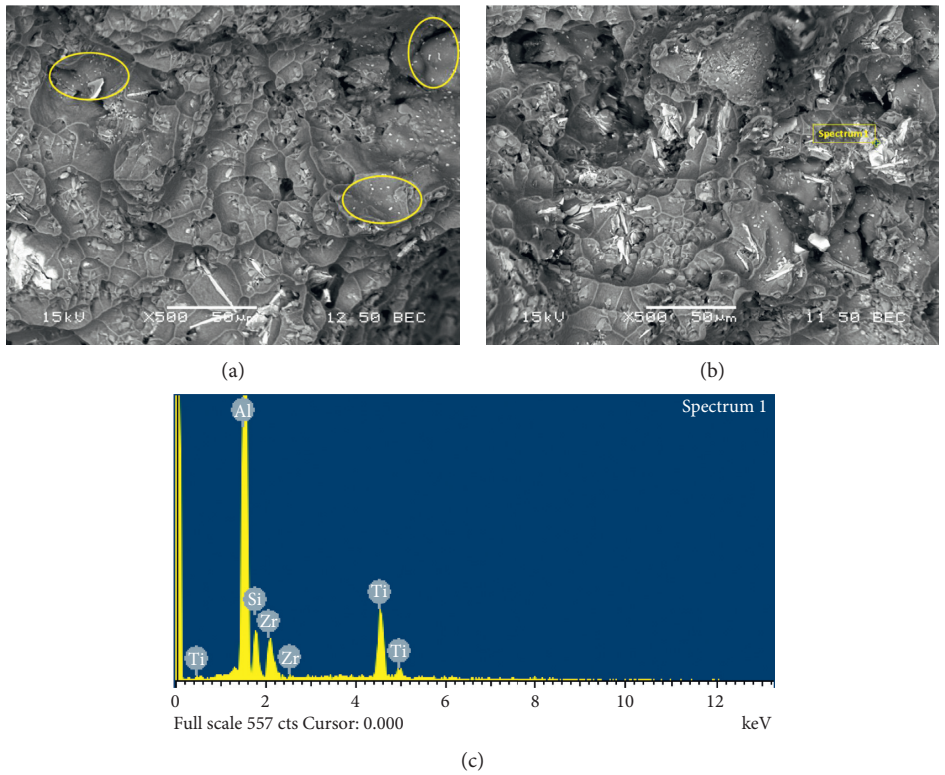

Figure 4: (a), (b) BSE images of T6-treated M1S alloy after stabilization at 250°C for 200 hours showing a coarse dimpled structure, coarsened precipitates, and Al_x (Zr, Ti)Si particles involved in the crack initiation process and (c) corresponding EDS spectrum of the phase of interest shown in (b).

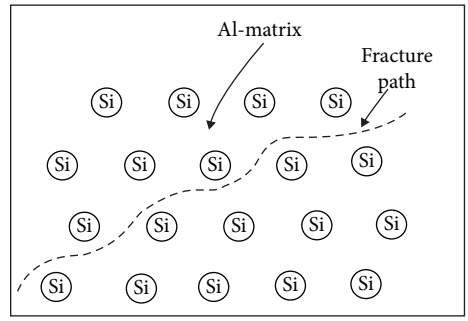

Figure 5: Fracture mechanism in Al-Si-Mg-based alloys [26].

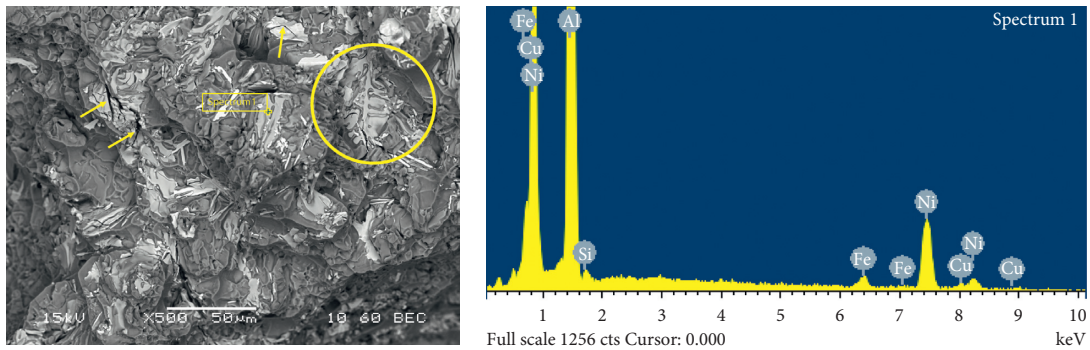

(a) (b)

Figure 6: SEM images of T6-treated M2S alloy after stabilization at 250°C for 1 hour: (a) BSE image showing microcracks associated with Ni-rich phases and (b) EDS spectrum corresponding to the point of interest in (a).

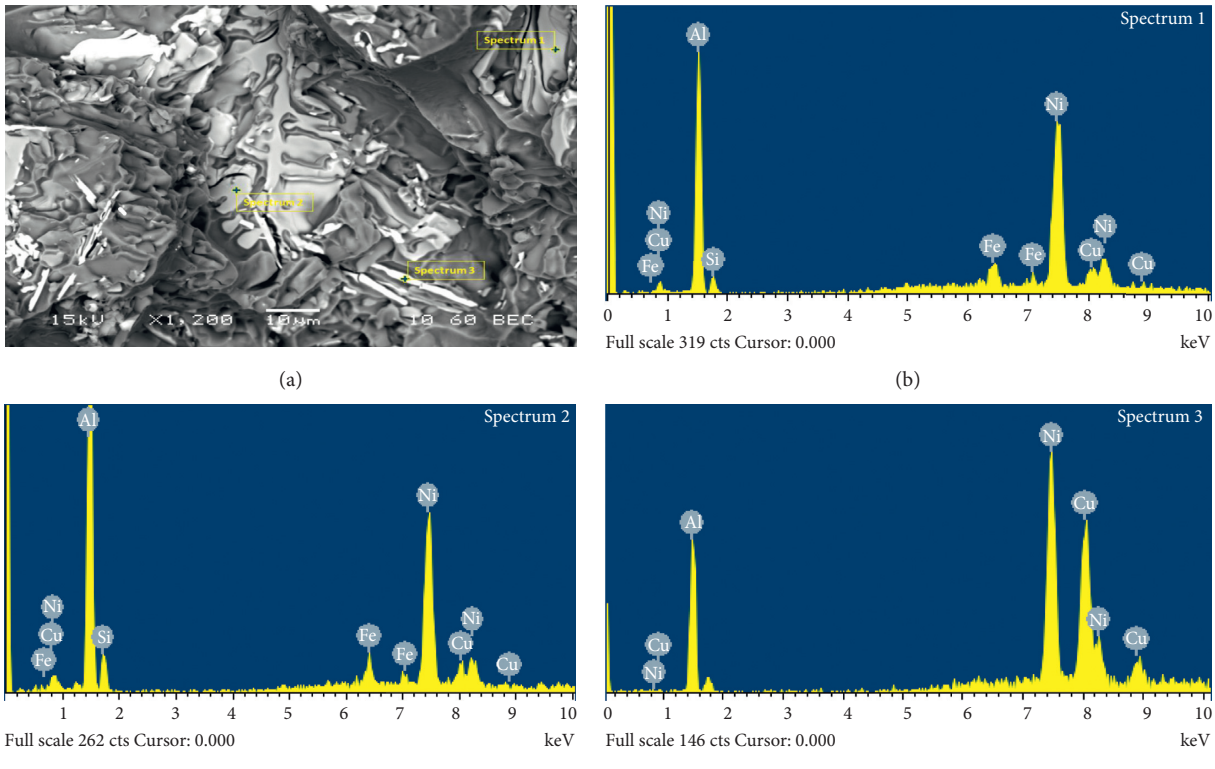

(a) (b) (c) (d)

Figure 7: (a) High magnification of the circled area shown in Figure 6 (a), (b) and (c), and (d) EDS spectra showing the chemical composition of the cracked phases in (a).

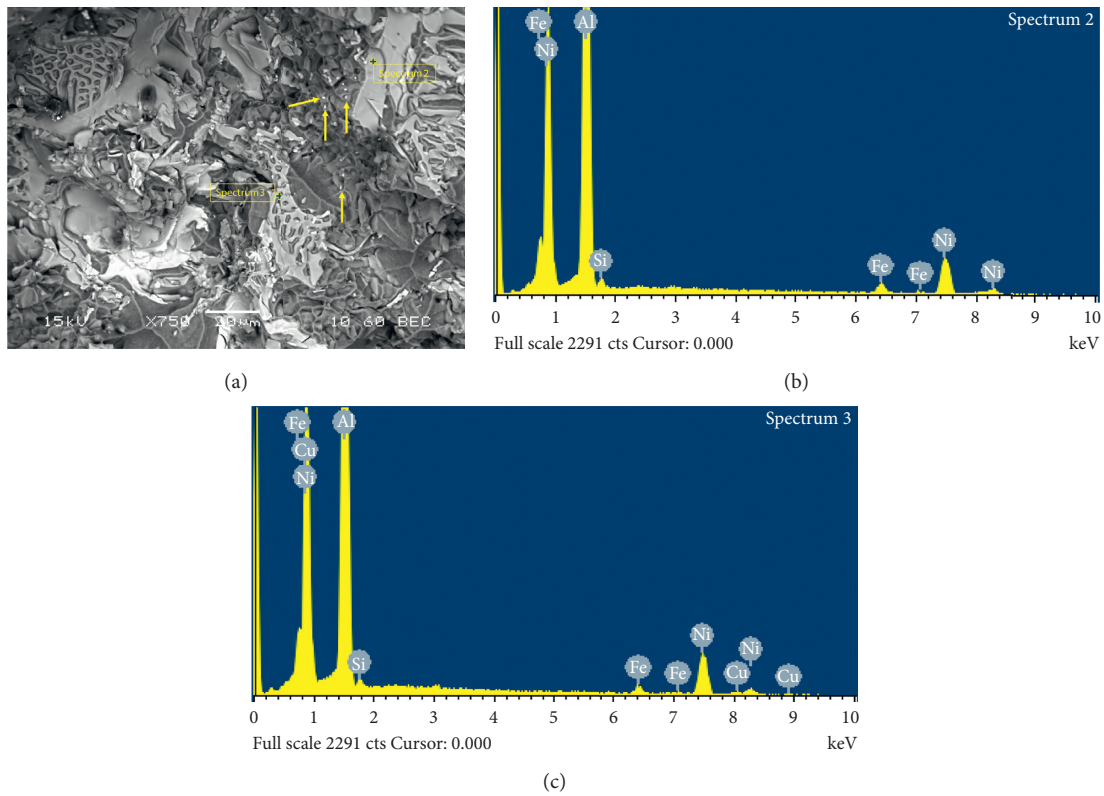

Figure 8: (a) BSE image of T6-treated M2S alloy after stabilization at 250°C for 200 hours showing the dimple structure, coarsened precipitates, and phases involved in the crack initiation process and (b), (c) EDS spectra identifying the Ni-rich phases shown in (a).

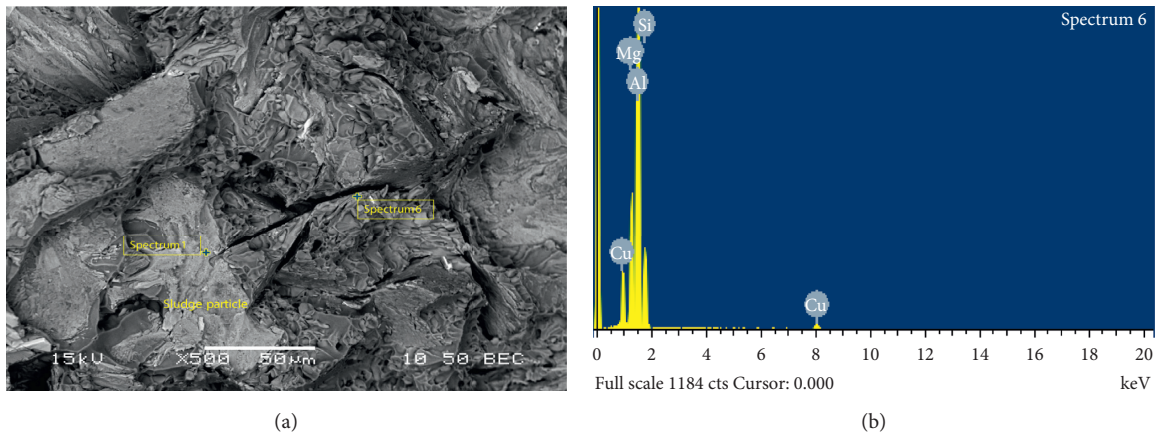

Figure 9: Continued.

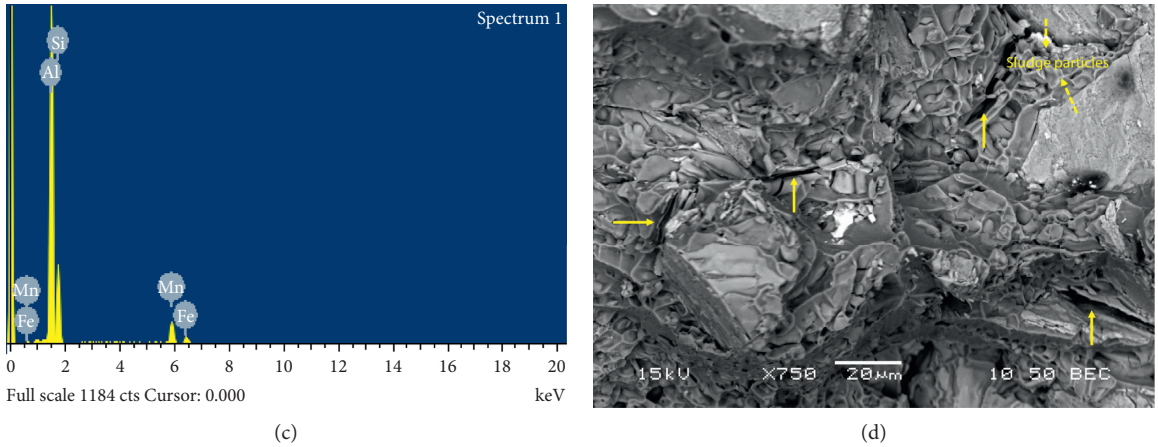

(c) (d)

FIGURE 9: SEM images of T6-treated M3S alloy after stabilization at 250°C for 1 hour: (a) BSE image showing a branched crack in a Q-phase particle and sludge particles preventing crack propagation, (b), (c) EDS spectra corresponding to the Q-phase and the sludge particle observed in (a), and (d) BSE image showing various cracked intermetallic phases and crack-free sludge particles.

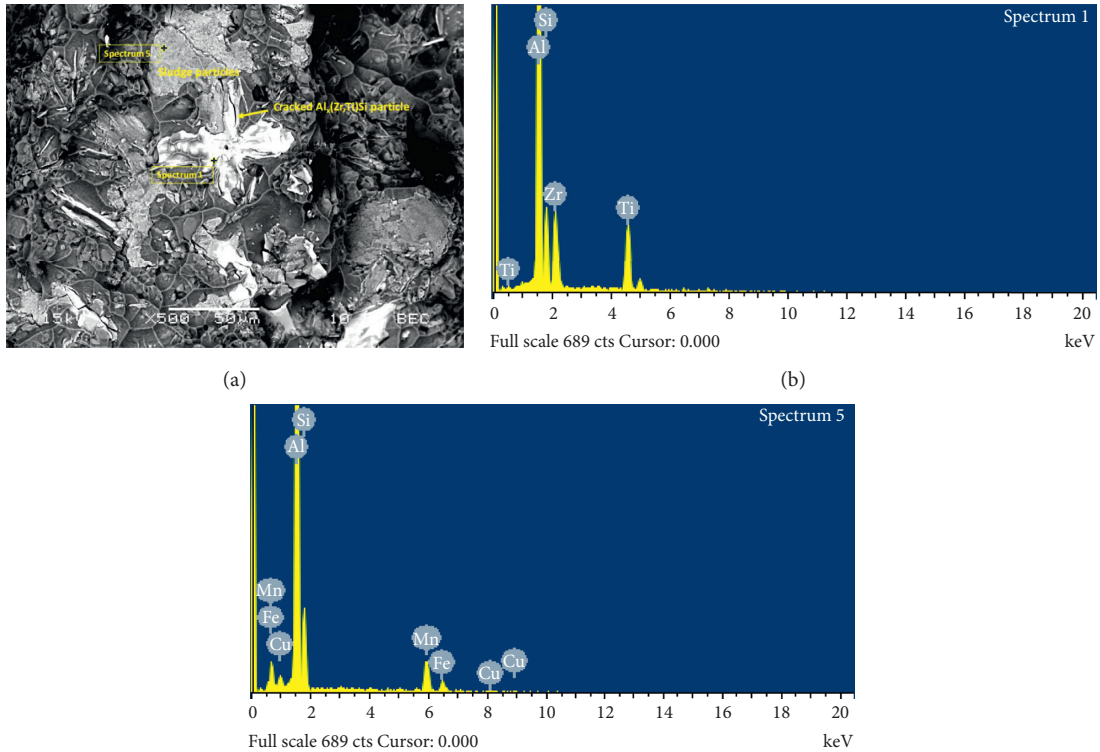

(a) (b)

(c)

FIGURE 10: (a) BSE image of T6-treated M3S alloy after stabilization at 250°C for 200 hours showing the dimple structure (upper right corner), coarsened precipitates and a cracked star-like Al-Si-Ti-Zr and sludge particles and (b), (c) EDS spectra corresponding to the Al-Si-Ti-Zr and sludge particles shown in (a).

compounds (referred to by the black arrow in Figure 12(a)). In both cases, the crack propagation was hindered by the elastic aluminum dendrites as indicated by the black circle in Figure 12(a). With the dramatic increase in the alloy ductility after stabilizing at 250°C for 200 h (i.e., UTS~91 MPa and %El~11), Figure 12(b) shows the elongated aluminum dendrites directed in the tensile direction with significant reduction in their size from about 25 μm to approximately 10 μm, which reflects the high ductility of the alloy.

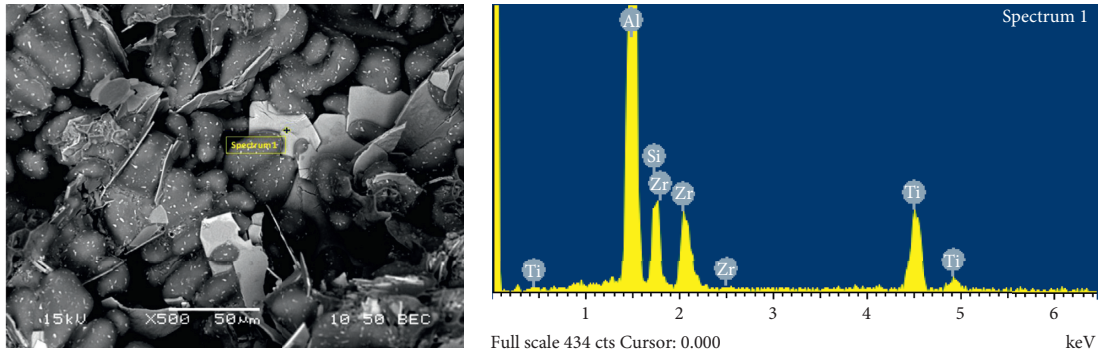

(a) (b)

Figure 11: (a) BSE image of T6-treated M3S alloy after stabilization at 250°C for 200 hours showing the distribution of coarsened precipitates and Al-Si-Ti-Zr thin plates and (b) EDS spectrum corresponding to the Al-Si-Ti-Zr plates observed in (a).

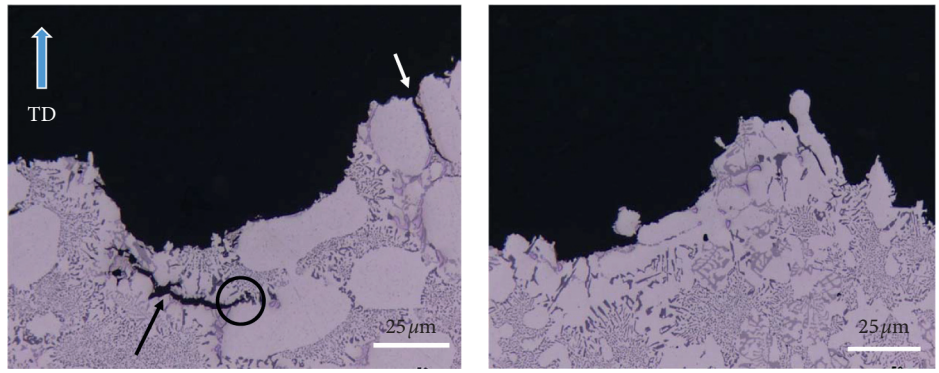

(a) (b)

Figure 12: Cross sections beneath the fracture surface of M1S alloy: (a) T6 condition and (b) after stabilization at 250 C for 200 h. The blue arrow indicates the tensile testing direction.

4. Summary

The main conclusions obtained from the present results can be summarized as follows:

(1) The Mn-containing alloy M3S exhibits higher ductility values at high temperature compared to the 2% Ni-containing alloys.

(2) The fracture surfaces of tested samples indicate the important role of sludge particles in enhancing the performance of Mn-containing alloys through their resistance to the propagation of cracks that developed in many intermetallic phases.

(3) The fracture surface of the T6-treated M1S alloy after stabilization for one hour at 250°C reveals a dimpled structure throughout, indicating the ductile nature of the fracture mode. The Al_x (Zr, Ti)Si complex compound is observed with star-like and blocky morphologies, with cracks appearing in various particles of this compound.

(4) By increasing the stabilization time up to 200 hours, coarser and deeper dimples are formed, highlighting the improved ductility of the alloy due to the softening behavior associated with the prolonged exposure at 250°C.

(5) In the one-hour stabilized T6-treated alloy M2S tested at 250°C, the appearance of microcracks in the Ni-rich phases, and the lower density of dimples on the fracture surface compared to those observed in the base alloy M1S emphasize the low ductility of alloy M2S with respect to alloy M1S.

Data Availability

Data will be made available upon request.

Conflicts of Interest

The authors declare that they have no conflicts of interest.

References

[1] Aluminum Association, *Aluminum: Properties and Physical Metallurgy*, ASM International, Cleveland, OH, USA, 1984.

[2] H. Ammar, *Influence of metallurgical parameters on the mechanical properties and quality indices of Al-Si-Cu-Mg and*

Al-Si-Mg casting alloys, PhD Dissertation, Université du Québec à Chicoutimi, Saguenay, Canada, 2010.

[3] R. C. Lemon and C. R. Howle, "Premium strength aluminum casting alloys 354 and 359," *Trans AFS*, vol. 70, pp. 465–470, 1963.

[4] J. G. Kaufman and E. L. Rooy, *Aluminum Alloy Castings: Properties, Processes and Applications*, ASM International, Cleveland, OH, USA, 2004.

[5] A. Couture, "Iron in aluminum casting alloys-a literature survey," *International Journal of Cast Metals Research*, vol. 6, no. 4, pp. 9–17, 1981.

[6] W. Bonsack, "Discussion on the effect of minor alloying elements on aluminum casting alloys," *ASTM Bulletin*, vol. 117, p. 45, 1942.

[7] J. Iglessis, C. Frantz, and M. Gantois, "Conditions de formation des phases de fer dans les alliages Al-Si de pureté commerciale," *Mémoires Scientifiques de la Revue de Métallurgie*, vol. 73, no. 4, pp. 237–242, 1977.

[8] ASM International, *ASM Handbook Volume 2: Properties and Selection: Nonferrous Alloys and Special-Purpose Materials*, ASM International, pp. 889–896, Cleveland, OH, USA, 1990.

[9] S. W. Nam and D. H. Lee, "The effect of Mn on the mechanical behavior of Al alloys," *Metals and Materials*, vol. 6, no. 1, pp. 13–16, 2000.

[10] D. H. Lee, J. H. Park, and S. W. Nam, "Enhancement of mechanical properties of Al-Mg-Si alloys by means of manganese dispersoids," *Materials Science and Technology*, vol. 15, no. 4, pp. 450–455, 1999.

[11] D. S. Park and S. W. Nam, "Effects of manganese dispersoid on the mechanical properties in Al-Zn-Mg alloys," *Journal of Materials Science*, vol. 30, no. 5, pp. 1313–1320, 1995.

[12] G. H. Garza-Elizondo, "Effect of Ni, Mn, Zr and Sc additions on the performance of Al-i-u-g alloys" Ph.D. Dissertation, Université du Québec à Chicoutimi, Saguenay, Canada, 2016.

[13] F. H. Samuel, A. M. Samuel, and H. Liu, "Effect of magnesium content on the ageing behaviour of water-chilled Al-Si-Cu-Mg-Fe-Mn (380) alloy castings," *Journal of Materials Science*, vol. 30, no. 10, pp. 2531–2540, 1995.

[14] M. H. Abdelaziz, H. W. Doty, S. Valtierra, and F. H. Samuel, "Mechanical performance of Zr-containing 354-type Al-Si-Cu-Mg cast alloy: role of additions and heat treatment," *Advances in Materials Science and Engineering*, vol. 2018, Article ID 5715819, 17 pages, 2018.

[15] M. H. Abdelaziz, E. M. Elgallad, H. W. Doty, S. Valtierra, and F. H. Samuel, "Melting and solidification characteristics of Zr-, Ni-, and Mn-containing 354-type Al-Si-Cu-Mg cast alloys," *Philosophical Magazine*, vol. 99, no. 13, pp. 1633–1655, 2019.

[16] M. H. Abdelaziz, A. M. Samuel, H. W. Doty, S. Valtierra, and F. H. Samuel, "Effect of additives on the microstructure and tensile properties of Al-Si alloys," *Journal of Materials Research and Technology*, vol. 8, no. 2, pp. 2255–2268, 2019.

[17] S. K. Shaha, "Development and characterization of cast modified Al-i-u-g Alloys for heat resistant power train applications" PhD Dissertation, Ryerson University, Toronto, Canada, 2015.

[18] K. E. Knipling, "Development of a Nanoscale Precipitation-Strengthened Creep-Resistant Aluminum Alloy Containing Trialuminide Precipitates," Northwestern University, Evanston, IL, USA, 2006.

[19] M. H. Abdelaziz, H. W. Doty, S. Valtierra, and F. H. Samuel, "Static versus dynamic thermal exposure of transition elements-containing Al-Si-Cu-Mg cast alloy," *Materials Science and Engineering: A*, vol. 739, pp. 499–512, 2019.

[20] D. Srinivasan and K. Chattopadhyay, "Metastable phase evolution and hardness of nanocrystalline Al-Si-Zr alloys," *Materials Science and Engineering: A*, vol. 304–306, pp. 534–539, 2001.

[21] Z. Yin, Q. Pan, Y. Zhang, and F. Jiang, "Effect of minor Sc and Zr on the microstructure and mechanical properties of Al-Mg based alloys," *Materials Science and Engineering: A*, vol. 280, no. 1, pp. 151–155, 2000.

[22] L. Alyaldin, M. H. Abdelaziz, A. M. Samuel, H. W. Doty, and F. H. Samuel, "Effect of transition metals addition on tensile properties of Al-Si-Cu-based alloys at 25°C and 250°C: role of heat treatment," *International Journal of Metalcasting*, pp. 1–16, 2020.

[23] A. R. Farkoosh, X. Grant Chen, and M. Pekguleryuz, "Interaction between molybdenum and manganese to form effective dispersoids in an Al-Si-Cu-Mg alloy and their influence on creep resistance," *Materials Science and Engineering: A*, vol. 627, pp. 127–138, 2015.

[24] Y. C. Chen, M. E. Fine, J. R. Weertman, and R. E. Lewis, "Coarsening behavior of Ll2 structured Al_3 (Zrx V1−x) precipitates in rapidly solidified Al-Zr-V alloy," *Scripta Metallurgica*, vol. 21, no. 7, pp. 1003–1008, 1987.

[25] Y. C. Chen, M. E. Fine, and J. R. Weertman, "Microstructural evolution and mechanical properties of rapidly solidified Al-Zr-V alloys at high temperatures," *Acta Metallurgica et Materialia*, vol. 38, no. 5, pp. 771–780, 1990.

[26] M. K. Surappa, E. W. Blank, and J. C. Jaquet, "Microstructural approach to deformation and fracture of cast Al-7Si-0.3 Mg," in *Proceedings of the 3rd International Conference on Solidification Processing*, pp. 424–427, Sheffield, UK, 1987.